Available online at www.sciencedirect.com
SCIENCE DIRECT
Polymer 46 (2005) 799–810
polymer
www.elsevier.com/locate/polymer

Bottom-up synthesis of PS–CNF nanocomposites

Yijin Xu, Bernadette Higgins, William J. Brittain*

Department of Polymer Science, The University of Akron, Akron, OH 44325-3909, USA

Received 1 August 2004; received in revised form 9 November 2004; accepted 16 November 2004
Available online 18 December 2004

Abstract

Polystyrene–carbon nanofiber (CNF) nanocomposites have been synthesized by a 'bottom-up' method through electrostatic assembly. First, a cationic polystyrene (PS) latex was synthesized by conventional emulsion polymerization. The latex was mixed with an aqueous suspension of oxidized CNF. PS–CNF nanocomposites were obtained by heterocoagulation due to the electrostatic interaction between cationic PS latex and anionic CNF. Thermal properties were characterized by DSC and TGA, while morphologies of the nanocomposites were studied by SEM. Electrical resistivity results showed that the percolation threshold in our PS–CNF nanocomposites was below 2 wt% (1 vol%). This low percolation threshold is related to the dispersion, and thus a superior network formation of CNF in PS matrix.

Keywords: Polystyrene–carbon nanofiber nanocomposites; Emulsion polymerization; Heterocoagulation

1. Introduction

Since the initial work of Iijima [1] for producing carbon nanotubes (CNTs), considerable research has been done in the field of polymer–CNT nanocomposites due to their superior mechanical and electrical properties [2–6]. Vapor grown carbon nanofibers (VGCFs), which typically have diameters in the range of 50–200 nm, are also referred to as multiwall CNTs. Compared with CNTs, especially with single wall carbon nanotubes, VGCFs can be produced today in higher volumes and at lower cost using natural gas or coal as the feed stock [7,8]. Their good thermal and electrical conductivity, excellent mechanical properties, high aspect ratio (up to 1000) and low cost have attracted attention from both industrial and academic areas [9–11].

One important application of CNF in polymer composites is mechanical reinforcement. Both thermoplastic and thermosetting polymers have been reinforced with CNFs: polypropylene (PP) [12–17], polycarbonate [18–20], poly (ether ether ketone) [21], nylon [17,22], ABS [23], and epoxy [24]. Conventional mixing methods such as a twin-screw extruder, high shear mixer and two-roll mill have been used. Another main application of CNFs exploits good electrical conductivity. An increasing number of components are being made from fiber reinforced composites. For example, aircraft radomes and the leading edge of the vertical stabilizers are generally made from glass fiber reinforced composites using an insulating polymer matrix. For these applications, some electrical conductivity is required to provide electrostatic dissipation (ESD) and electromagnetic-radio frequency interference (EMI/RFI) protection. Currently, a highly conductive filler such as carbon black is added to the matrix in order to ensure electrical conductivity above the required level; this approach reduces the manufacturing and maintenance costs of components as compared with those previously coated with an anti-static paint [25–27]. In order to obtain a conductive path throughout a component, a 3-dimensional network of conductive filler particles is required, which is known as percolation. The percolation threshold is the filler loading at which the electrical resistance of the composite sharply drops. Both theoretical and experimental results indicate that the percolation threshold strongly depends on the particle shape, the higher the aspect ratio, the lower the percolation threshold [28,29]. Due to a high aspect ratio (up to 1000) and good electrical conductivity, CNFs are a good choice among carbon fibers for applications in ESD, EMI and RFI [30,31]. For the preparation of PP–CNFs

* Corresponding author. Fax: +1 330 972 5290.
E-mail address: wjbritt@uakron.edu (W.J. Brittain).

0032-3861/$ - see front matter © 2004 Published by Elsevier Ltd.
doi:10.1016/j.polymer.2004.11.091

nanocomposites, the first step was melt mixing PP and CNFs followed by compression or injection molding. By compressing molding, Lozano et al. [32] reported a 9–18 wt% percolation threshold. Using injection molding, Gordeyev and coworkers [33] obtained PP–CNF nanocomposites with a percolation threshold around 4% in volume (given that the specific gravity is about 2 g/cm^3, this is equivalent to 8 wt%). In Andrade's work [34], a percolation threshold as low as 1% in volume (about 2 wt%) was reported, but there was no description about the preparation method. We cannot reconcile these differences at this time, but the difference might be due to the alignment during injection process or the surface chemistry of CNFs. In the preparation of epoxy-CNF nanocomposites, Prasse et al. [35] reported a percolation threshold as low as 0.75 wt% with the help of electric field induced alignment during curing and the nanocomposites were electrically anisotropic. Enomoto and coworkers [36] prepared CNF–polystyrene (PS) nanocomposites by injection molding; the percolation threshold is about 3–4% in volume (6–8 wt%). In polymer blend-CNF systems, the Sumita group [37] found that CNF selectively locates within one polymer phase and forms a network structure at a rather low concentration. In a poly(methyl methacrylate) (PMMA)/high density polyethylene (HDPE)–CNF system, the percolation threshold of PMMA–CNF reduced from 8 to 4 wt% with the addition of 1% of HDPE, and this threshold further reduced to 1.5 wt% after the specimens were annealed at 220 °C for 30 min. In all the systems reviewed above, high shear and relatively long mixing times were used in order to separate CNFs and disperse CNFs in the polymer matrix. One result of the high shear mixing is that the CNFs are broken and thus the aspect ratio is reduced which directly affects the percolation threshold and load transfer [18,28].

In this paper we report the 'bottom-up' synthesis of PS–CNF nanocomposites by a heterocoagulation method. Heterocoagulation is a general method which is widely used in preparing organic/organic, organic/inorganic and inorganic/inorganic hybrids [38–43]. Recently we have successfully synthesized polymer–clay nanocomposites with fully exfoliated morphology by this method [44,45]. The mechanism of this route is ion exchange between cationic PS latex and oxidized CNF; the PS latex particles deposited onto the surface of CNF due to ionic bonding. The merits of the present method include: easy regulation of CNF loading, no shear (cost-effective and maintains high aspect ratio), and no solvent (environment friendly).

2. Experimental section

2.1. Materials

2, 2′-Azobis (2-amidinopropane) dihydrochloride (V-50), provided by Wako Pure Chemical Industries Ltd., was used without further purification. Cetyltrimethylammonium bromide (CTABr) and sodium hydroxide were obtained from Aldrich and used as received. Styrene (St) from Aldrich was purified by distillation under vacuum before use. Deionized water was used in all the experiments. The vapor grown carbon nanofiber (VGCNFs) is Pyrograf III® PR-19-PS from Applied Sciences, Inc. (ASI) with diameters of about 200 nm and length of 100–200 μm. This CNF was oxidized by ASI with approximately 5% surface oxygen content; the oxygen functionality is a mixture of carboxylic, carbonyl, lactonic, hydroxyl and ether-type groups.

2.2. Preparation of cationic polystyrene (PS) latex

Into a four-necked 500 mL Pyrex reaction kettle, which was equipped with a mechanical stirrer, argon inlet, refluxing condenser and a dropping funnel for the addition of St monomer, were placed 250 mL of deionized water, 15 g of purified St, 1 g of CTABr, and 0.76 g of V-50. The reaction contents and St in dropping funnel were purged with argon for 45 min. The polymerization was commenced by heating at 60 °C while stirring at 300 rpm. 35 g of St monomer was added dropwise to the reaction kettle over 3 h. After the addition of St, the polymerization temperature was maintained at 70 °C for 100 min and then the mixture was cooled to room temperature. Some latex was taken out to determine monomer conversion by a gravimetric method.

2.3. Cation exchange of CNFs

To convert the carboxylic acid groups on the CNF surface into sodium carboxylate groups, the oxidized CNF was treated with sodium hydroxide. A typical procedure is as follows. 0.5 g of CNF was dispersed in 100 mL of 1 M aqueous NaOH solution and sonicated for 1 h, then CNF followed by filtration and repeated washing with deionized water. Finally the cation exchanged CNF was redispersed in deionized water and sonicated before mixing with cationic PS latex.

2.4. Heterocoagulation of PS latex with CNFs

A predetermined amount of cationic latex and CNF suspension were mixed together in a beaker with stirring. The mixture was stirred for 3 h and then allowed to stand overnight. The colloidal mixture was demulsified by freezing at −20 °C; after thawing to room temperature, the mixture was filtered and thoroughly washed with water. The nanocomposite was collected and dried at 70 °C in vacuo until constant weight was obtained. For scanning electron microscopy (SEM) studies, the colloid mixture was collected at different times after mixing and diluted with deionized water; a drop of the diluted colloid was deposited on an aluminum foil and allowed to dry for SEM examination.

2.5. Sample preparation by compression molding

For electrical resistivity determination, the dry nanocomposite powder was compression molded into a sheet with the dimensions of 7 cm in length, 2.5 cm in width and 0.8 cm in thickness. To study the effect of molding conditions on the electrical resistivity and percolation threshold of nanocomposites, different molding temperatures and pressures were used. A known amount of nanocomposite powder was put into the mold, pressed at 35 MPa at 150 °C for 15 min; then the mold was removed and cooled with water. The specimen was dried at 80 °C overnight and stored in a desiccator for electrical resistivity and thermal property testing. After these measurements, the sheet was remolded under a pressure of 25 MPa at 185 °C for 20 min; while for dynamic mechanical thermal analysis (DMTA), the specimens are 15 mm long, 5 mm wide and 0.75 mm thick. The samples for TGA and DSC measurements were taken from the remolded specimens.

2.6. Instrumentation

Thermogravimetric analysis (TGA) was performed on a Hi-Res TGA 2950 thermograimetic analyzer (TA instruments) in the temperature range of 25–800 °C and at a heating rate of 20 °C/min in air atmosphere. Differential scanning calorimetry (DSC) experiment was run on a TA Instruments DSC 2920 Modulated DSC under a nitrogen atmosphere. A hermetically sealed sample was heated from 25 to 180 °C at the ramping rate of 10 °C/min; after the first run it was removed and quickly cooled to room temperature. We report the results from second run in this paper. DMTA experiments were performed on a Rheometric Scientific TM (DMTA V) in bending configuration at the frequency of 1 Hz, the temperature was raised from 25 to 150 °C at a ramping rate of 2 °C/min under nitrogen atmosphere. Scanning electron microscopy (SEM) was performed to investigate the heterocoagulation process and the morphology of the nanocomposite with a JEOL JSM-5300 Scanning Microscope. The molded specimens were frozen in liquid nitrogen, fractured, mounted, and coated with gold/platinum using a SPI Sputter™ (Model 12121, SPI Supplies Division of Structure Probe, Inc.). The electrical resistivity was measured by standard four point method; silver paste was used to ensure good contact between the sample surface and copper electrodes. The applied voltage for the measurement was 1 V.

3. Results and discussion

For the purposes of reinforcement and electrical conductivity, CNTs and CNFs must be well dispersed in the polymer matrix and there should be good adhesion between nanofillers and polymer matrix. Because of their unique structures, there is no good solvent for either CNTs or CNFs, which is the biggest obstacle in preparing well-dispersed polymer–CNT and -CNF nanocomposites. To solve this problem, different methods have been used to modify CNTs to make them soluble in common solvents or miscible with the polymer matrix or to generate suitable functional groups on the CNT surface for further derivation [46]. In the case of CNFs, traditional treatments such as electrochemical, wet chemical and air oxidation or coating with polymers have been pursued [47]. Surface oxidation has been used to provide the CNF surface with carboxylic groups, which can be used to increase the interaction between CNFs and a polymer matrix or for further functionalization [48].

The extrusion or milling process, generally used in polymer–CNF nanocomposites preparation, will break the CNFs and reduce the aspect ratio of CNF [12–23,33]. Barraza et al. [49] prepared PS- and poly(styrene-*co*-isoprene)-CWNT nanocomposites by miniemulsion polymerization. The electrical resistivities of the PS–SWCT nanocomposites are very high: at 3.5–4 wt% SWCT loading, ρ is higher than $2E+16\ \Omega\cdot cm$; at 8.5 wt% SWCT loading, $\rho = 7.47E+6\ \Omega\cdot cm$. Considering the small average diameter of 1.2–1.3 nm and the high surface area, it is likely that the SWCTs are not well dispersed in the PS matrix. Alternatively, Dufresne and coworkers [50] prepared CNT-poly(styrene-*co*-butyl acrylate) nanocomposites by a heterocoagulation method. They solubilized CNT with the anionic surfactant sodium dodecyl sulfate (SDS) and mixed this aqueous suspension with the cationic latex. The percolation threshold of the nanocomposites was about 1.5 vol% (about 3 wt%), which is relatively high considering the small diameter of CNT (30–50 nm). The main shortcoming of these nanocomposites is that there is poor adhesion between CNT and the polymer matrix.

3.1. Heterocoagulation

The heterocoagulation method is widely used in preparing organic/organic, organic/inorganic and inorganic/inorganic hybrids [38–43]. We have successfully prepared exfoliated polymer–clay nanocomposites by this method [44,45]. This method has been used to modify negatively charged pulp fibers with cationic latex for some time. The ionic interaction at the fiber–polymer interface contributes much to the adhesion between fiber and polymer matrix [51].

Here, we report the synthesis of PS–CNF nanocomposites by the heterocoagulation method. The CNFs we used in this experiment were oxidized to generate carboxylic groups on the CNF surface, which was confirmed by characteristic absorption around $1730\ cm^{-1}$ in FTIR spectrum. We sonicated the oxygenated CNF in an aqueous solution of NaOH to convert the –COOH groups on CNF surface to $-COO^{-}Na^{+}$ groups, which will interact with quaternary ammonium and amidinium cations on the surface of cationic PS latex.

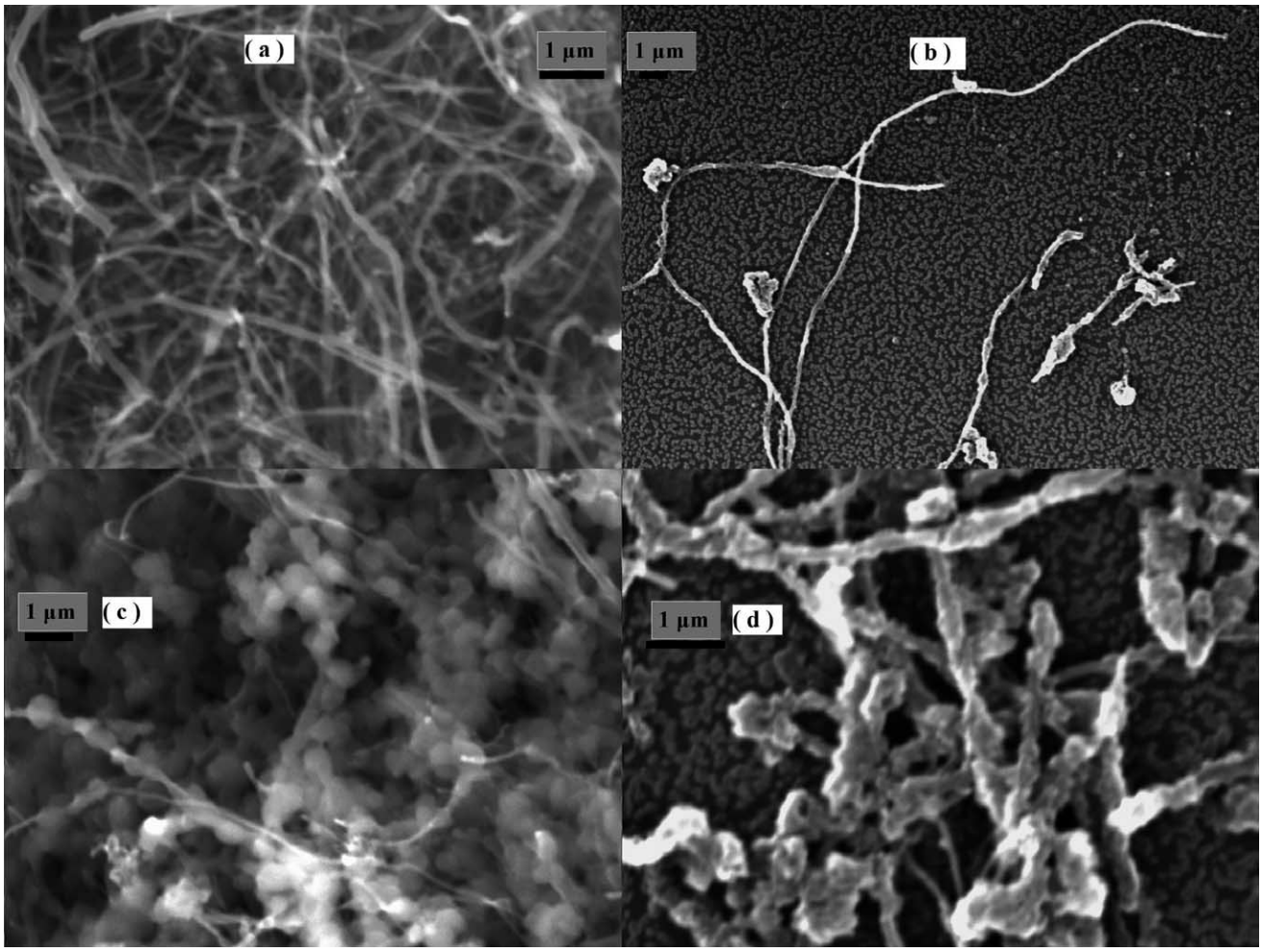

Fig. 1. SEM pictures of pristine CNF (a), 5 min after mixing (b), 12 h after mixing (d) and nanocomposite powder after freeze-deemulsification and drying (10.6% CNF loading) (c); (a) and (c) were not coated with gold–platinum.

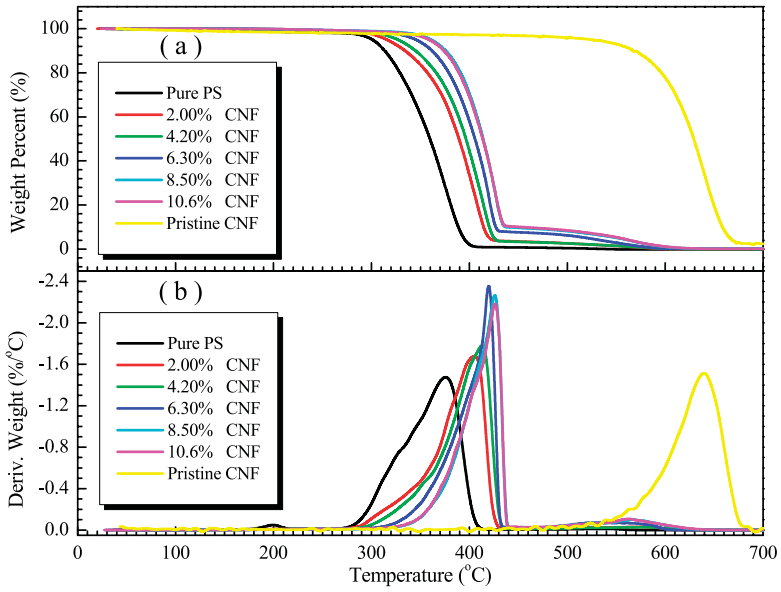

Fig. 2. TGA and DTG profiles of PS, pristine CNF and PS–CNF nanocomposites.

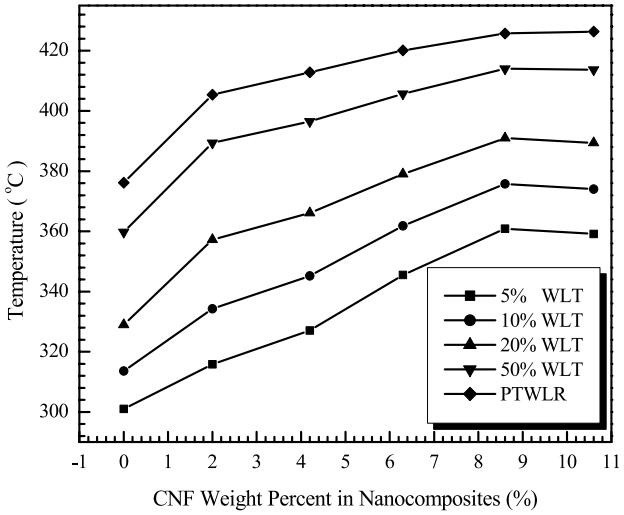

Fig. 3. Effects of CNF loadings on weight loss temperature (WLT) and the peak temperature of weight loss rate (PTWLR) for PS–CNF nanocomposites.

Fig. 1(a)–(d) depict the SEM pictures of pristine CNF (a), a colloidal mixture after 5 min and 12 h mixing (b and d), and the dried nanocomposite powder before compression molding (c). From SEM, the average diameters of CNFs and cationic PS latex are 200 and 120 nm. From the picture of sample taken 5 min after mixing (Fig. 1(b)), we can see a few PS latex particles deposited on the CNF surface, but after 12 h (Fig. 1(d)) most of the CNF surface was covered with PS latex and it is obvious that coalescence of the PS latex has occurred. It is interesting that the CNFs were held together by the PS coagulum. Fig. 1(c) was taken of the nanocomposite powder after freeze-deemulsification and drying; the coalescence of the PS latex is clearly observed. Some CNF is fully covered with PS and some are just partially covered. Based on Fig. 1(b)–(d), we speculate that

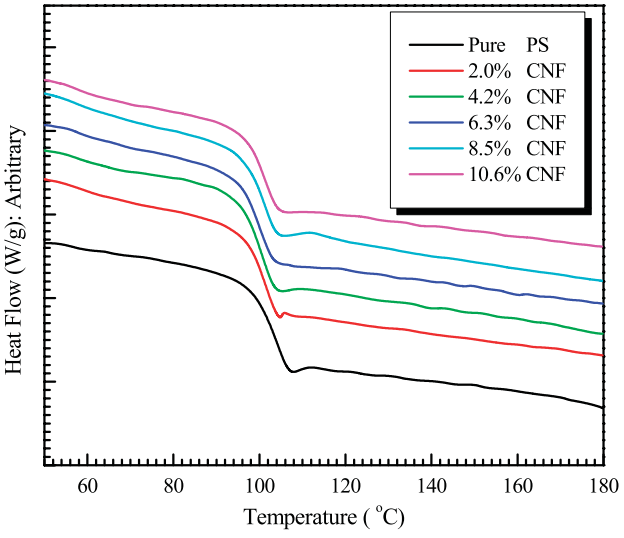

Fig. 4. DSC thermograms of PS–CNF nanocomposites at different CNF loadings.

single PS latex particles deposit on CNF surface through electrostatic interactions followed by PS latex coalescence due to environmental changes (such as the release of NaCl from ion exchange) or the freeze-deemulsification process. We believe that the ionic interaction between CNF and PS will improve the interfacial adhesion and load transfer from PS matrix to CNFs. The reason why some CNFs are just partially coated with PS latex may be due to the low carboxylic group content on CNF surface and the inhomogeneity of carboxylic group distribution on CNF surface. The surface oxygen content by XPS is only about 5% and these oxygen atoms are a mixture of functionalities [48].

3.2. Thermal and dynamic mechanical thermal properties of PS–CNF nanocomposites

Fig. 2(a) shows the thermo-oxidative degradation profiles of pure PS, pristine CNF and PS–CNF nanocomposites; Fig. 2(b) shows the DTG curves from the same TGA analyses. It can be seen that the addition of CNF increases the onset temperature and end temperature of PS decomposition in the PS–CNF nanocomposites. At lower CNF loadings the increase is more significant and there is no visible difference between PS–CNF nanocomposites with 8.5 and 10.6% CNF loadings. From Fig. 2(b) we can see that there is a shoulder peak on the main weight loss rate curve at lower temperatures; with increasing CNF loading, this peak disappears and the peak temperature of weight loss rate and the end temperature of PS decomposition shifts to higher values. In some polymer–CNF and polymer–CNT nanocomposites, this kind of increase was also observed and was attributed to restrictions on macromolecule mobility imposed by CNFs [16,52,53]. It is interesting that the CNF in the nanocomposites decomposes at lower temperatures compared to pristine CNF (Fig. 1(b)). This has not been reported before.

To more clearly show the effect of CNF on the thermo-oxidative stability of PS–CNF nanocomposites, Fig. 3 summarizes the temperatures for 5, 10, 20 and 50% weight loss as well as the peak temperature of weight loss rate (PTWLR) at different CNF loadings. The temperatures at 5, 10 and 20% weight loss increased by 60 °C; while for 50% weight loss and PTWLR, the temperatures increased by 54 and 50 °C. 5% WLTs increase almost linearly with CNF loadings, but the increases of 10, 20 and 50% WLTs and PTWLR from 0 to 2% CNF loadings are much greater than those from 2 to 8.5% CNF loadings. This may be due to the restrictions on the mobility of macromolecules imposed by CNFs and the relatively high viscosity of nanocomposite melt at lower temperatures, which results in more difficult vaporization of small molecules due to PS degradation. The difference among 5, 10, 20 and 50% WLTs decreases with increasing of CNF loadings.

There are few reports about the effects of CNF on glass transition temperatures (T_g) of polymer–CNT and polymer–CNF nanocomposites. Thostenson and Chou [54] reported a

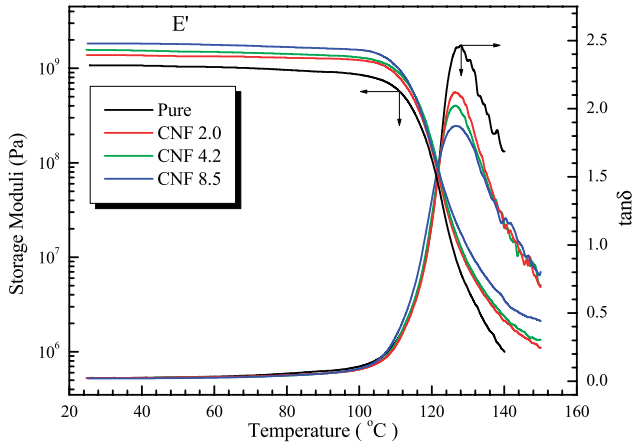

Fig. 5. DMTA of PS–CNF nanocomposites as function of CNF loading and temperature.

increase of T_g in PS–CNT nanocomposites with 5 wt% CNT loading, while Dufresne and coworkers [50] found no effect of CNT on the T_g of CNT–poly(styrene-*co*-butyl acrylate) nanocomposites at CNF loadings up to 15 wt%. Our DSC results also suggest no effect of CNF on the T_gs of PS–CNF nanocomposites up to 10.6 wt% CNF loading, as shown in Fig. 4.

The elastic modulus and damping properties of the PS–CNF nanocomposites were characterized by DMTA as a function of both CNF loading and temperature. Fig. 5 shows an increase with CNF loadings both below and above the glass transition temperature (about 127 °C). Like the results obtained from DSC, the glass transition temperature itself was not affected as shown by the peak position of the tangent of the ratio of loss to storage modulus (tan δ), a measure of the damping within the system. The decreasing height of the peak with increasing CNF loading is due to the reduced fraction of polymer-matrix.

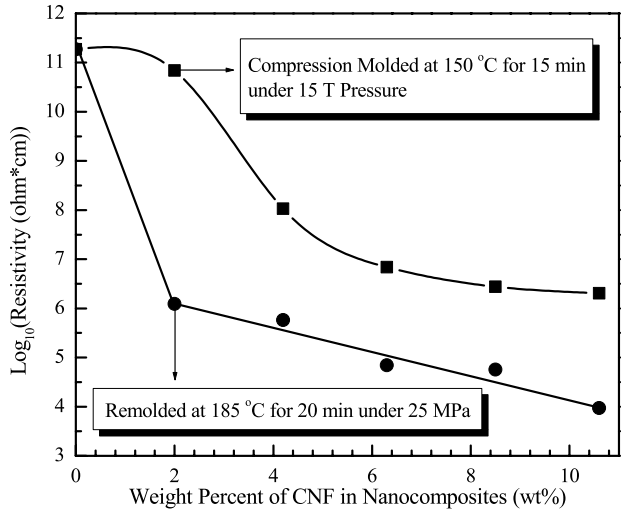

Fig. 6. Dependence of electrical resisitivity of PS–CNF nanocomposites on molding conditions.

3.3. Electrical resistivity of PS–CNF nanocomposites

In the preparation of CNT- and CNF–polymer nanocomposites, a major challenge is to homogeneously disperse CNTs and CNFs in the polymer matrix. To make the nanocomposite conductive, a network of CNTs and CNFs should be formed. The electrical resistivity will drop sharply at the percolation threshold. Fig. 6 shows the electrical resistivity change for the PS–CNF nanocomposites. When the nanocomposites were compression molded at 150 °C under a pressure of 35 MPa for 15 min, we can see that the electrical resistivity dropped sharply at 2 wt% (1 vol%) CNF loading. At 10.6 wt% (~5 vol%) CNF loading, the electrical resistivity of 2.04E+6 Ω cm is five orders of magnitude smaller than PS. At this point, the nanocomposite is a semiconductor [55]. When the specimens were remolded at higher temperature and longer times (185 °C under a pressure of 25 MPa for 20 min), a further decrease of electrical resistivity for the nanocomposites was observed. At 2 wt% CNF loading, the decrease is of five orders of magnitude and after 2 wt%, the resistivity continuously decreases with the increase of CNF loadings and it is below 1E+4 at 10.6 wt% (about 5 vol%) CNF loading. Compared with the percolation thresholds of reported polymer–CNF nanocomposites [32–34,36,37], Barraza's [49] result suggested that single wall CNTs are not well dispersed because the resistivity of their nanocomposites were high, even though the diameter of their single wall CNTs is 1.2–1.3 nm, which provides more surface area. The percolation threshold of CNT-poly (styrene-*co*-butyl acrylate) nanocomposites reported by Dufresne and coworkers [50] is about 1.5 vol% (3 wt%) CNT loading; considering the smaller diameter of their CNTs (30–50 nm) to the 200 nm diameter of our CNFs, our percolation threshold is lower.

The effect of molding conditions on electrical conductivity has been observed before [56]. At lower molding temperatures, the viscosity is relatively high and it is difficult for CNFs to move and form network structures. The higher molding temperature and times lowers the percolation threshold. Also high pressure is often used to decrease the void content in specimen.

3.4. Morphology study by scanning electronic microscopy (SEM)

In previous section, we showed that molding conditions greatly affect the conductivity behavior of PS–CNF nanocomposites. To better understand this phenomenon, we studied the fracture surface of these nanocomposite specimens by SEM.

3.4.1. Morphology of PS–CNF nanocomposites molded at 150 °C

Fig. 7(a) and (b) are typical surface morphologies of the PS–CNF nanocomposites at 2.0 and 10.6 wt% CNF loading

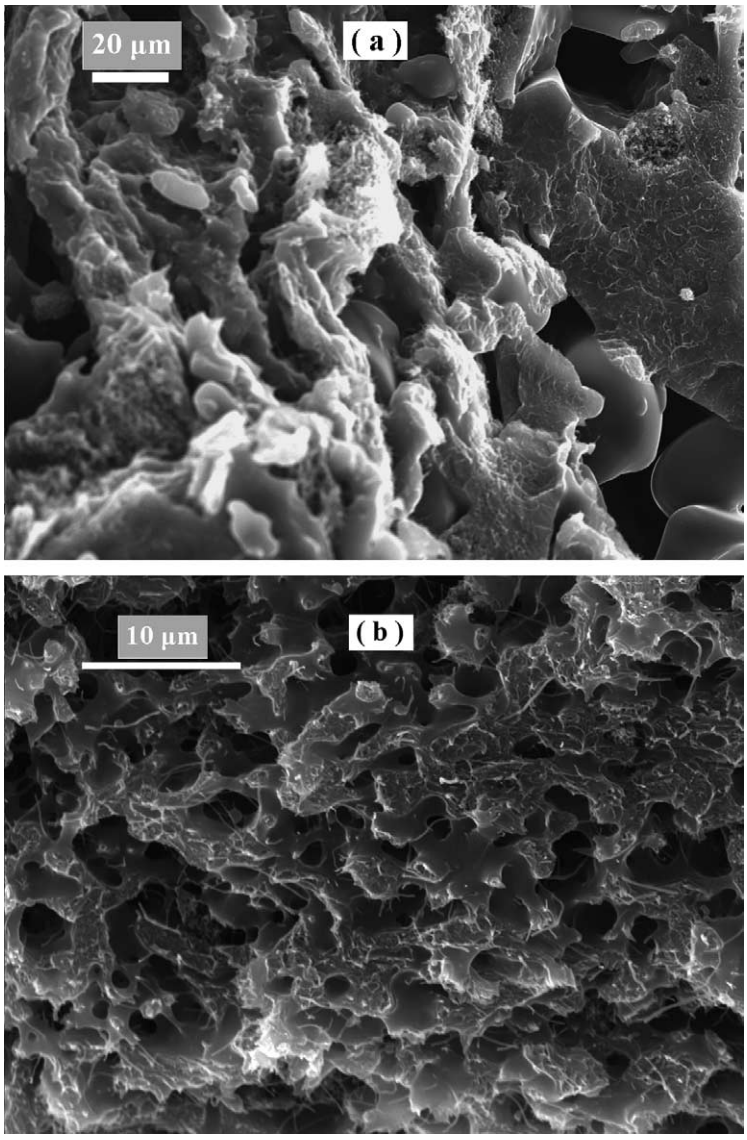

Fig. 7. SEM picture of PS–CNF nanocompoiste at 2.0 wt% (a) and 10.6 wt% (b) CNF loadings molded at 150 °C under a pressure of 35 MPa for 15 min.

respectively for molding at 35 MPa for 15 min. From both pictures we can see that there are voids in the specimens, which suggests that the mobility of both CNFs and PS macromolecules are restricted at this molding temperature due to the high viscosity of nanocomposite melts. This is reflected in the electrical resistivity data. Fig. 8(a)–(c) are informative. First, there is good wettability between the CNF and PS, the reason that CNFs are not completely covered with PS particles is probably due to a low carboxylic group concentration on the CNF surface. Second, the PS particles and PS coagulum act as an adhesive that holds the CNFs together resulting in the formation of CNF networks. In a previous report, Zhou [57] believed that the presence of polymer particles on CNTs was due to the polymer matrix fracture, we believe that this CNF-stringing-through-the particle structure is not due to the fracture of polymer matrix, because we do not observe this structure after the nanocomposites were remolded at higher temperatures.

3.4.2. Morphology of PS–CNF nanocomposites remolded at 185 °C

Fig. 9(a)–(c) show low magnification SEM images of the morphologies of fracture surfaces of remolded PS–CNF nanocomposites at 2.0, 4.2, and 10.6 wt% CNF loadings for molding at 25 MPa and 20 min. The images clearly show that with increasing CNF loading, the fracture surface of nanocomposite becomes rougher. This is reasonable in terms of CNF reinforcement because the rougher the fracture surface represents a higher fracture energy. We do not observe any voids in the remolded specimens; this indicates the importance of proper molding conditions for preparing nanocomposite specimens.

From Fig. 6, we can see that the resistivity of the

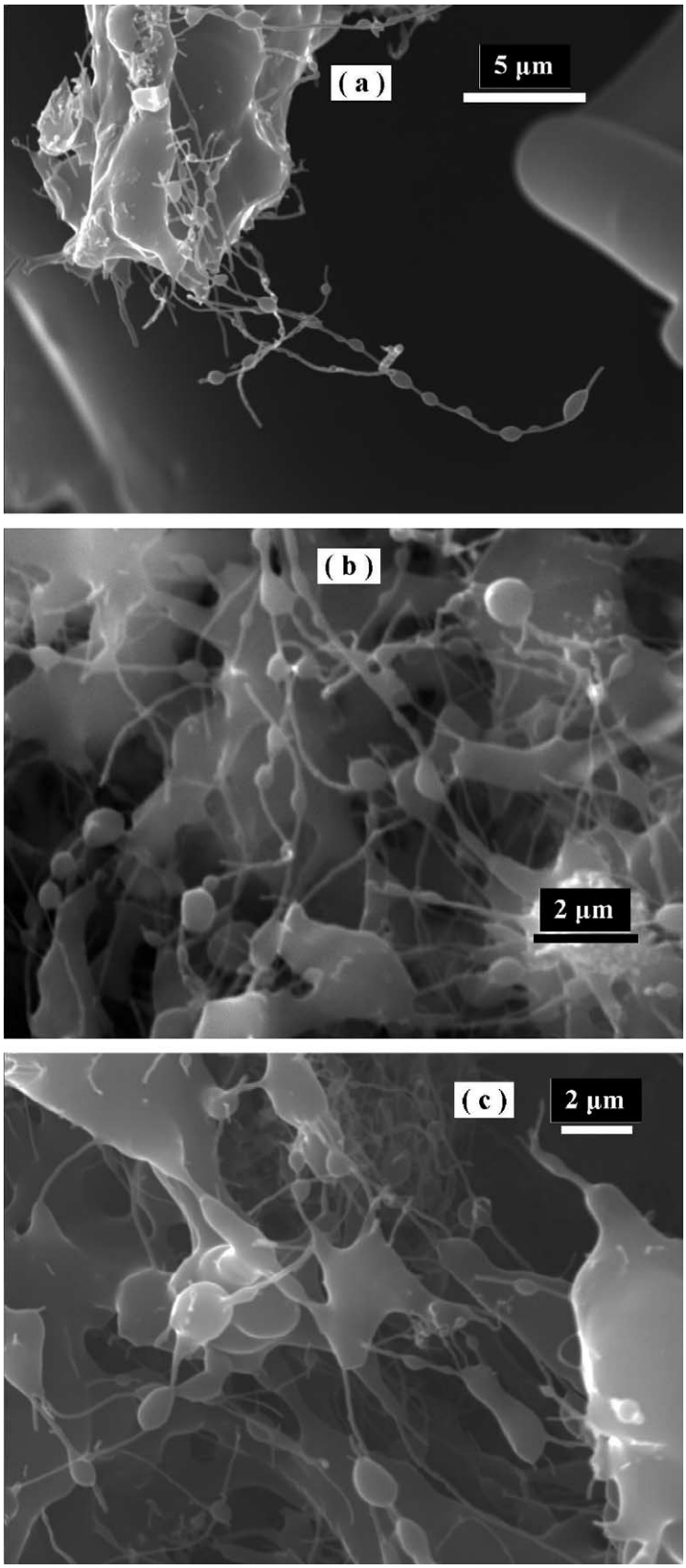

Fig. 8. SEM evidence of CNF–PS wettability and CNF networks in nanocomposites at 2.0 wt% (a), 4.2 wt% (b) and 10.6 wt% CNF loadings. The specimens were molded at 150 °C under a pressure of 35 MPa for 15 min.

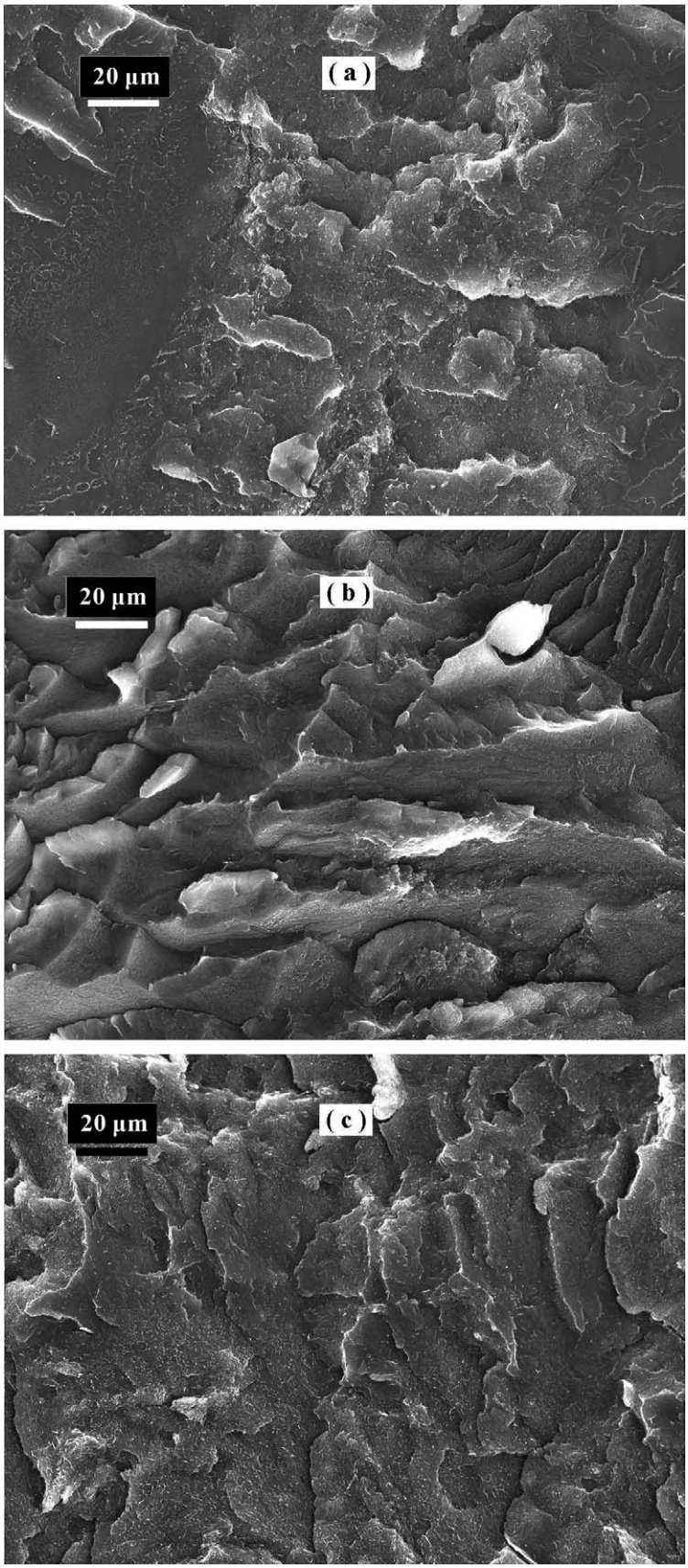

Fig. 9. Low magnification SEM images of PS–CNF nanocomposites of 2.0 wt% (a), 4.2 wt% (b) and 10.6 wt% (c) CNF loadings. The specimens were remolded at 185 °C under a pressure of 25 MPa for 20 min.

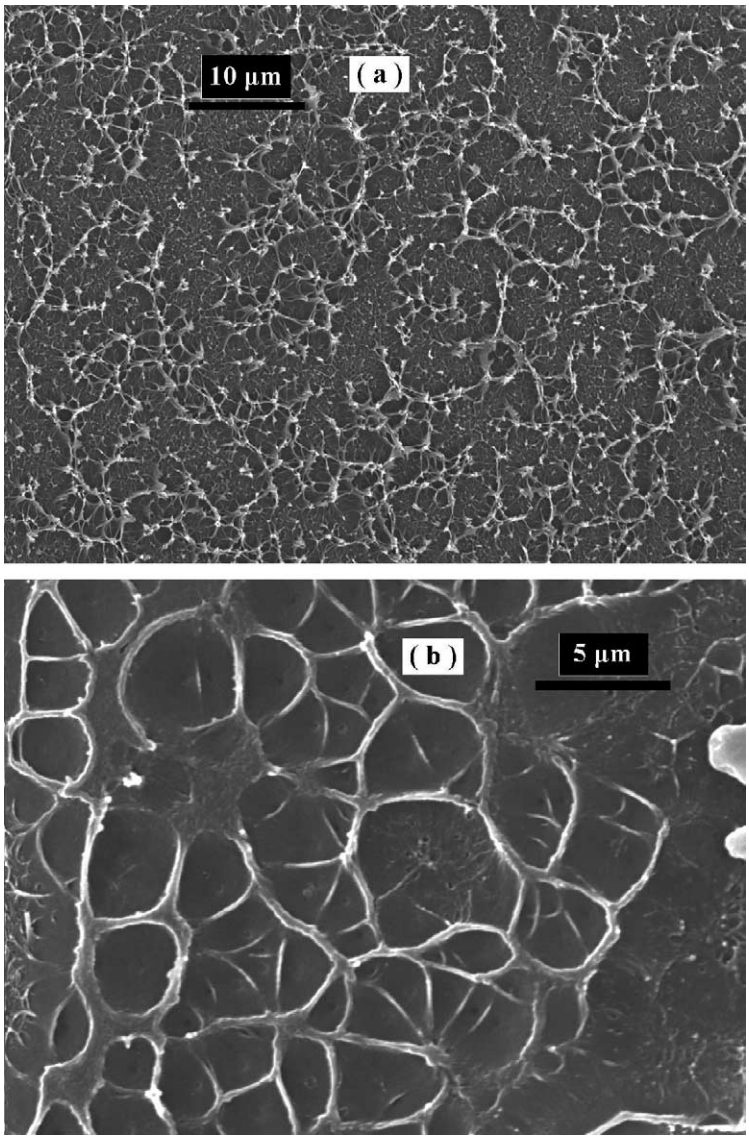

Fig. 10. SEM evidence of CNF network formation in PS–CNF nanocomposite (2.0 wt% CNF loading). The specimen was remolded at 185 °C under a pressure of 25 MPa for 20 min.

remolded nanocomposites at 2.0 wt% CNF loading decreased five orders of magnitude. To explain this phenomenon, we examined the surface morphologies of remolded specimens. Fig. 10(a) is a typical SEM picture of PS–CNF nanocomposite at 2.0 wt% CNF loading, it shows the formation of CNF network with no voids. Fig. 10(b) shows the network structure at higher magnification. For all the nanocomposites, the network form is almost the same but the dimension varies. This network formation is the reason for a dramatic conductivity increase. From Fig. 8, we believe that the CNFs are held together by PS, but the reason why CNFs can bend and form that kind of network is not clear at this moment.

In the study of polymer–fiber composites, the load transfer is a very important issue. Good interfacial adhesion will favor load transfer from the polymer matrix to fibril filler resulting in the reinforcement. Fig. 10 shows the typical surface morphology. The white spots in Figs. 10(a) and (b), and 11(a) and (b) are broken CNF ends; the length of the CNF projecting from the fracture surface is less than 1 μm. Because the typical length of the CNF we used was higher than 100 μm, so we can assume that the CNF at the fractured surface is not due to the pull-out of CNF from PS matrix, but due to broken CNFs. In combination with the information in Fig. 10, we believe that the fracture happened in PS matrix as well as broken CNFs. This type of fracture indicates the successful transfer of load from the PS matrix to CNF, which shows the importance of CNF surface modification and PS–CNF interfacial interaction.

4. Summary

We successfully prepared PS–CNF nanocomposites by a

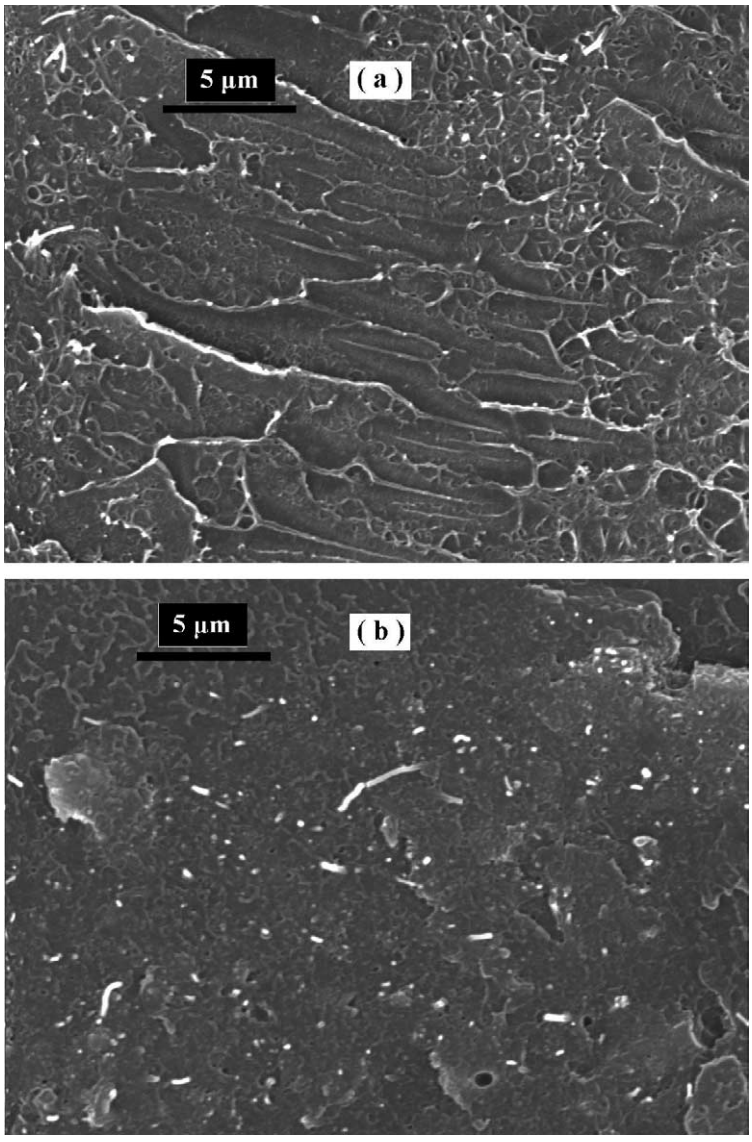

Fig. 11. SEM images of PS–CNF nanocomposites: (a) and (c) 2.0 wt% and (b) 5.0 wt% CNF loading. The specimens were remolded at 185 °C under a pressure of 25 MPa for 20 min.

heterocoagulation method through electrostatic assembly between a cationic PS latex and a negatively charged CNF. The presence of CNF increases the onset and end thermo-oxidative decomposition temperature by about 60 °C but has no effect on the glass transition temperature. Molding temperature has a significant effect on the morphology of and the electrical conductivity of PS–CNF nanocomposites. When the PS–CNF nanocomposites are molded at 185 °C under a pressure of 25 MPa for 20 min, the percolation threshold is below 2 wt% (1 vol%) CNF loading, which is the best result obtained for polymer–CNF nanocomposites. The presence of carboxylic groups on the CNF surface enhances the interfacial adhesion and load transfer, resulting in PS matrix damage during the fracture process. We believe that this method can also be extended to polymer–CNT systems [48e].

Acknowledgements

This research was supported by the DURINT on Microstructure, Processing and Mechanical Performance of Polymer Nanocomposites, Air Force Contract No F49620-01-1-0447.

References

[1] Iijima S. Nature 1991;354:56.
[2] Lau KT, Hui D. Compos: Part B 2002;33:263.
[3] Thostenson EJ, Ren Z, Chou TW. Compos Sci Technol 2001;61:1899.
[4] Salvetat JP, Kulik AJ, Bonard JM, Briggs GAD, Stockli T, Metenier K, Bonnamy S, Beguin F, Burnham NA, Forro L. Adv Mater 1999;11:161.
[5] Wong EW, Sheehan PE, Lieber CM. Science 1997;277:1971.

[6] Treacy MMJ, Ebbesen TW, Gibson JM. Nature 1996;381:678.
[7] Tarasen WL, Alig R, Glasgow G, Jacobsen R. Pyrograf-III®: VGCF nanofibers for Engineered Composites, Prograf Products Inc. report.
[8] Rodriquez NM. J Mater Res 1993;8:3233.
[9] Heremans J, Beetz Jr. CP. Phys Rev B 1985;32:1981.
[10] Heremans J. Carbon 1985;23:431.
[11] Endo M, Kim YA, Hayashi T, Nishimura K, Matusita T, Miyashita K, Dresselhaus MS. Carbon 2001;39:1287.
[12] Finegan IC, Tibbetts GG, Gibson RF. Compos Sci Technol 2003;63: 1629.
[13] Kuriger RJ, Alam MK, Anderson DP, Jacobsen RL. Compos: Part A 2002;33:53.
[14] Cooper CA, Ravich D, Lips D, Mayer J, Wagner HD. Comp Sci Technol 2002;62:1105.
[15] Kumar S, Doshi H, Srinivasarao M, Park JO, Schiraldi DA. Polymer 2002;43:1701.
[16] Lozano K, Barrera EV. J Appl Polym Sci 2001;79:125.
[17] Tibbetts GG, McHugh JJ. J Mater Res 1999;14:2871.
[18] Ma H, Zeng J, Realff ML, Kumar S, Schiraldi DA. Compos Sci Technol 2003;63:1617.
[19] Takahashi T, Yonetake K, Koyama K, Kikuchi T. Macromol Rapid Commun 2003;24:763.
[20] Carneiro OS, Covas JA, Bernardo CA, Caldeira G, Van Hattum FWJ, Ting JM, Alig RL, Lake ML. Compos Sci Technol 1998;58:401.
[21] (a) Sandler J, Werner P, Shaffer MSP, Demchuk V, Altstadt V, Windle AH. Compos: Part A 2002;33:1033.
(b) Sandler J, Windle AH, Werner P, Altstadt V, ES MV, Shaffer MSP. J Mater Sci 2003;38:2135.
[22] Pogue RT, Ye J, Klosterman DA, Glass AS, Chartoff RP. Compos: Part A 1998;29A:1273.
[23] Shui X, Chung DDL. Proc 38th Inter SAMPE Symp 1993;1869.
[24] (a) Patton RD, Pittman Jr. CU, Wang L, Hill JR. Compos: Part A 1999;30A:1081.
(b) Richard P, Prasse T, Cavaille L, Chazeau L, Gauthier C, Duchet J. Mater Sci Eng 2003;A352:344.
[25] Shaffer MSP, Windle AH. Adv Mater 1999;11:937.
[26] Makela T, Sten J, Hujanen A, Isotalo H. Synth Met 1999;101:707.
[27] Chandrasekhar P, Naishadham K. Synth Met 1999;105:115.
[28] Munson-McGee SH. Phys Rev B 1991;43:3331.
[29] Celzard A, McRae E, et al. Phys Rev B 1996;53:6209.
[30] Lee BO, Woo WJ, Kim MS. Macromol Mater Eng 2001;286:114.
[31] Sandler J, Shaffer MSP, Prasse T, Bauhofer W, Schulte K, Windle AH. Polymer 1999;40:5967.
[32] Lozano K, Bonilla-Rois J, Barrera EV. J Appl Polym Sci 2001;80: 1162.
[33] Gordeyev SA, Macedo FJ, Ferreira JA, Van Hattum FWJ, Bernardo CA. Physica B 2000;279:33.
[34] Andrade Jr. JS, Kobayashi Y, Shibusa Y, Shirane K. Physica A 1998; 248:227.
[35] Prasse T, Cavaille JY, Bauhofer W. Compos Sci Technol 2003;63: 1835.
[36] Enomoto K, Yasuhara T, Kato K, Ohtake N. Nippon Kikai Gakkai Ronbunshu 2003;69:1145.
[37] Wu G, Asai S, Sumita M. Macromolecules 1999;32:3534.
[38] Furusawa K. In: Esumi K, editor. Polymer interfaces and emulsions. New York, Marcel Dekker, Inc., New York, p. 129.
[39] Maroto JA, de las Nieves F. J Colloids Surf A 1995;96:121.
[40] Islam AM, Chowdhry BZ, Snowden MJ. Adv Colloid Interface Sci 1995;62:109.
[41] Lagaly G, Mecking O, Penner D. Colloid Polym Sci 2001;279:1090 see also p. 1097.
[42] Rossi GB, Beaucage G, Dang TD, Vaia RA. Nano Lett 2002;2:319.
[43] Kolny J, Kornowski A, Weller H. Nano Lett 2002;2:361.
[44] Huang X, Brittain WJ. Macromolecules 2001;34:3255.
[45] Xu YJ, Brittain WJ, Xue CC, Eby RK. Polymer 2004;45:3735.
[46] (a) Sun YP, Fu K, Lin Y, Huang W. Acc Chem Res 2002;35:1096.
(b) Niyogi S, Hamon MA, Hu H, Zhao B, Bhowmik P, Sen R, Itkis ME, Haddon RC. Acc Chem Res 2002;35:1105.
(c) Banerjee S, Kahn MGC, Wong SS. Chem Eur J 2003;9:1898.
(d) Tasis D, Tagmatarchis N, Georgakilas V, Prato M. Chem Eur J 2003;9:4000.
[47] Peng JCM, Donnet JB, Wang TK, Rebouillat S. In: Donnet JB, Wang TK, Peng JCM, Rebouillat S, editors. Carbon Fibers. New York Marcel Dekker Inc., New York. Chapter 3.
[48] (a) Ros TG, Van Dillen AJ, Genus JW, Koningsberger DC. Chem Eur J 2002;8:1151.
(b) Paredes JI, Martinez-Alonso A, Tascon JMD. Carbon 2002;40: 1101.
(c) Toebes ML, Van Heeswijk JMP, Bitter JH, Jos Van Dillen A, de Jong KP. Carbon 2004;42:307.
(d) Brandl W, Marginean G, Chirila V, Warschewski W. Carbon 2004;42:5.
[49] Barraza HJ, Pompeo F, O'Rear EA, Resasco DE. Nano Lett 2002;2: 797.
[50] Dufresne A, Paillet M, Putaux JL. J Mater Sci 2002;37:3915.
[51] Alince B, Arnoldova P, Frolik R. J Appl Polym Sci 2000;76:1677.
[52] Ahmad MY, Mustafah J, Mansor M, Mohd Ishak ZA, Mohd Omar AK. Polym Int 1995;38:1.
[53] Jin Z, Pramoda KP, Xu G, Goh SH. Chem Phys Lett 2001;337:43.
[54] Thostenson EK, Chou TW. J Phys D: Appl Phys 2002;35:L77.
[55] Hummelin RE. Electronic properties of materials. 3rd ed. New York: Springer; 2001, p. 78.
[56] Zhang C, Yi XS, Asai S, Sumita M. Comp Interface 1999;6:287.
[57] Jin L, Bower C, Zhou O. Appl Phys Lett 1998;73:1197.